Charge density wave with meronlike spin texture induced by a lateral superlattice in a two-dimensional electron gas

R. Côté and Xavier Bazier-Matte
Département de physique, Université de Sherbrooke, Sherbrooke, Québec J1K 2R1, Canada
(Received 12 July 2016; revised manuscript received 23 August 2016; published 7 November 2016)

The combined effect of a lateral square superlattice potential and the Coulomb interaction on the ground state of a two-dimensional electron gas in a perpendicular magnetic field is studied for different rational values of Γ, the inverse of the number of flux quanta per unit cell of the external potential, at filling factor $\nu = 1$ in Landau-level $N = 0$. When Landau-level mixing and disorder effects are neglected, increasing the strength W_0 of the potential induces a transition at a critical strength of $W_0^{(c)}$ from a uniform and fully spin-polarized state to a two-dimensional charge density wave (CDW) with a meronlike spin texture at each maximum and minimum of the CDW. The collective excitations of this "vortex CDW" are similar to those of the Skyrme crystal that is expected to be the ground-state *near* filling factor $\nu = 1$. In particular, a broken $U(1)$ symmetry in the vortex CDW results in an extra gapless phase mode that could provide a fast channel for the relaxation of nuclear spins. The average spin-polarization S_z changes in a continuous or discontinuous manner as W_0 is increased depending on whether $\Gamma \in [1/2,1]$ or $\Gamma \in [0,1/2]$. The phase mode and the meronlike spin texture disappear at a large value of W_0 leaving as the ground state a partially spin-polarized CDW if $\Gamma \neq 1/2$ or a spin-unpolarized CDW if $\Gamma = 1/2$.

DOI: 10.1103/PhysRevB.94.205303

I. INTRODUCTION

The two-dimensional electron gas (2DEG) in a perpendicular magnetic field has a very rich phase diagram that includes several phases, such as the Laughlin liquids that give rise to the integer and quantum Hall effects [1], the Wigner crystal at a small filling factor in each Landau level [2,3], the bubble crystals and the stripe phase in higher Landau levels [4], and the Skyrme crystal [5,6] near-filling factor $\nu = 1$ in the lowest Landau level. The phase diagram is even more complex when systems with extra degrees of freedom, such as double-quantum wells (DQWs), are considered [7]. In DQWs, the orientation of the pseudospin vector associated with the layer degree of freedom can be modified by changing the tunneling and electrical bias between the layers.

Another way to modify the properties of the 2DEG is by the addition of a lateral two-dimensional superlattice patterned on top of the GaAs/AlGaAs heterojunction hosting the 2DEG that creates a spatially modulated potential at the position of the 2DEG [8]. The effect of a one-dimensional periodic potential on the Landau levels is particularly interesting [9,10] since it leads to commensurability problems due to the presence of different length scales: the lattice constant of the external potential a_0, the magnetic length $\ell = \sqrt{\hbar c/eB}$ (B is the magnetic field), and the Fermi wavelength. Novel magnetoresistance oscillations with periods different than that of the well-known Shubnikov–de Haas oscillations have been detected in such systems. Even more interesting is the effect of a periodic two-dimensional potential on the band structure of the 2DEG [11–13]. The intricate pattern of eigenvalues that results from such a potential has been studied by many authors and is known as the Hofstadter butterfly spectrum [14]. Its observation in the GaAs/AlGaAs heterojunction is very difficult due to screening and disorder effects, but experimental signatures in magnetotransport experiments in 2DEGs with lateral surface superlattice potentials with periods on the order of 100 nm and less have been reported [15–17]. Interest in this problem has been revived recently by the experimental observations of Hofstadter's butterfly spectrum that uses the moiré superlattices that arise from graphene or bilayer graphene placed on top of the hexagonal boron nitride [18,19]. Another interest of superlattice potentials is their use to create artificial lattices. For example, a lateral superlattice with a honeycomb crystal structure has recently been proposed to create an artificial graphenelike system [20,21] in a GaAs/AlGaAs heterojunction.

In this paper, we study theoretically the effect of a square lattice lateral potential with a period a_0 on the ground state of the 2DEG in the GaAs/AlGaAs heterojunction at filling factor $\nu = 1$ and in Landau-level $N = 0$. We include the spin degree of freedom and use the Hartree-Fock approximation to study the combined effects of the external potential and the Coulomb interaction. We assume that the potential is sufficiently weak so that Landau-level mixing can be neglected. We also ignore disorder and work at zero temperature. We vary the potential strength W_0 and calculate the ground state for different rational values of $\Gamma = \varphi_0/Ba_0^2 = q/p \in [0,1]$ (where $\varphi_0 = hc/e$ is the flux quantum and q, p are integers with no common factors) which is the inverse of the number of flux quanta per unit cell of the surface potential. Our formalism allows for the formation of uniform as well as spatially modulated ground states with or without spin texture. Our calculation indicates that, at a critical value of $W_0^{(c)}$ of the external potential, there is a transition from a uniform fully spin polarized state to a charge density wave (CDW) with an intricate spin texture. Each unit cell of this CDW contains two positive and two negative amplitude modulations, and the vortex spin texture at each maximum (minimum) resembles that of a positively (negatively) charged meron. The two positively (negatively) charged merons in each unit cell have the same vorticity but a global phase that differs by π. These meronlike textures, however, are not quantized since the amplitude of the CDW varies continuously with W_0. In the vortex CDW, as we call it, the average spin-polarization S_z varies with W_0 in a

continuous or discontinuous manner depending on whether $\Gamma \in [1/2,1]$ or $\Gamma \in [0,1/2]$ and saturates at a finite positive value of S_z that depends only on Γ in most cases. In the special case of $\Gamma = 1/2$, the vortex-CDW phase is absent, and the transition is directly from a fully spin-polarized and uniform 2DEG to an unpolarized CDW. The phase diagram for $\Gamma \in [0,1/2]$ is richer than that of $\Gamma \in [1/2,1]$ as it involves the transition between the vortex CDW and its conjugate phase, the antivortex CDW, obtained by reversing $S_z(\mathbf{r})$ and inverting the vorticity of all merons. This transition between the two CDWs is accompanied by a discontinuous change in S_z that becomes continuous when the Zeeman coupling goes to zero.

We study the properties of the vortex CDW at different values of Γ and with a particular emphasis on its collective excitations which we derive using the generalized random-phase approximation (GRPA). The vortex CDW has collective modes that have much in common with the collective excitations of the Skyrme crystal [22] that is expected to be the ground-state near-filling factor $\nu = 1$ in $N = 0$. Namely, the broken $U(1)$ symmetry in the vortex-CDW phase leads to a new gapless mode that can provide a fast channel for the relaxation of nuclear spins [23]. This mode and the meronlike spin texture disappear at larger values of the external potential leaving a ground state that is either unpolarized if $\Gamma = 1/2$ or partially polarized if $\Gamma \neq 1/2$.

Our paper is organized as follows. In Sec. II, we introduce the Hamiltonian of the 2DEG in the presence of the lateral square lattice potential and briefly review the Hartree-Fock and generalized random-phase approximation that we use to compute the density of states, the density, the spin profiles, and the collective excitations of the various phases. In Sec. III, we present our numerical results for the phase diagram of the 2DEG as a function of the potential strength W_0 and the inverse magnetic flux per unit cell Γ. We conclude in Sec. IV with a discussion on the experimental detection of the new vortex-CDW state.

II. HAMILTONIAN OF THE 2DEG IN AN EXTERNAL POTENTIAL

The system we consider is a 2DEG in a GaAs/AlGaAs heterojunction or quantum well submitted to a perpendicular magnetic-field $\mathbf{B} = B\hat{\mathbf{z}}$ and to a lateral superlattice potential $V_e(\mathbf{r})$. The coupling of the electrons to this external potential is given by $H_e = -e\int d\mathbf{r}\, V_e(\mathbf{r})n_e(\mathbf{r})$, where $n_e(\mathbf{r}) = \sum_{\alpha=\pm} n_{e,\alpha}(\mathbf{r})$ is the total density operator including both spin states $\alpha = \pm 1$ (we take $e > 0$). We assume that only the Landau-level $N = 0$ is occupied but our calculation can easily be generalized to any Landau level by changing the effective interactions $H(\mathbf{q})$ and $X(\mathbf{q})$ and the form factor $F(\mathbf{q})$. The Hamiltonian of the interacting 2DEG is given in the Hartree-Fock approximation by

$$\begin{aligned} H_{HF} = &-N_\varphi \frac{\Delta_Z}{2}\sum_\alpha \alpha\rho_{\alpha,\alpha}(0) \\ &- \frac{eN_\varphi}{S}\sum_{\mathbf{q}}\sum_\alpha V_e(-\mathbf{q})F(-\mathbf{q})\rho_{\alpha,\alpha}(\mathbf{q}) \\ &+ N_\varphi \sum_{\alpha,\beta}\sum_{\mathbf{q}\neq 0} H(\mathbf{q})\langle\rho_{\alpha,\alpha}(-\mathbf{q})\rangle\rho_{\beta,\beta}(\mathbf{q}) \\ &- N_\varphi \sum_{\alpha,\beta}\sum_{\mathbf{q}} X(\mathbf{q})\langle\rho_{\alpha,\beta}(-\mathbf{q})\rangle\rho_{\beta,\alpha}(\mathbf{q}), \end{aligned} \tag{1}$$

where S is the 2DEG area, $N_\varphi = S/2\pi\ell^2$ is the Landau-level degeneracy, and the form factor for the $N = 0$ Landau level is

$$F(\mathbf{q}) = e^{-q^2\ell^2/2}, \tag{2}$$

where $\ell = \sqrt{\hbar c/eB}$ is the magnetic length. The averages are over the Hartree-Fock ground state of the 2DEG. The noninteracting single-particle energies, measured with respect to the kinetic-energy $\hbar\omega_c/2$, are given by

$$E_\alpha = \alpha\frac{\Delta_Z}{2}, \tag{3}$$

where the Zeeman energy is $\Delta_Z = |g^*|\mu_B B$ with g^* as the effective g factor of bulk GaAs and μ_B is the Bohr magneton. In some experiments on skyrmions, the effective g factor was tuned in the range of -0.11 to 0.065 by applying hydrostatic pressure to a sample of a GaAs/AlGaAs modulation-doped quantum well [24]. In our paper, we will thus consider that Δ_Z is not determined by the magnetic field but is instead a parameter than can be adjusted.

The Hartree and Fock interactions in $N = 0$ are given by

$$\begin{aligned} H(\mathbf{q}) &= \left(\frac{e^2}{\kappa\ell}\right)\frac{1}{q\ell}e^{-q^2\ell^2/2}, \\ X(\mathbf{q}) &= \left(\frac{e^2}{\kappa\ell}\right)\sqrt{2}\int_0^\infty dx\, e^{-x^2}J_0(\sqrt{2}xq\ell), \end{aligned} \tag{4}$$

where $\kappa = 12.9$ is the dielectric constant of GaAs. Finally, the operators $\rho_{\alpha,\beta}(\mathbf{q})$ are defined by

$$\rho_{\alpha,\beta}(\mathbf{q}) \equiv \frac{1}{N_\varphi}\sum_{X,X'} e^{-(i/2)q_x(X+X')}\delta_{X,X'+q_y\ell^2}c^\dagger_{X,\alpha}c_{X',\beta}, \tag{5}$$

where $c^\dagger_{X,\alpha}$ is the operator that creates an electron with guiding-center index X (in the Landau gauge) and spin α. The four operators $\rho_{\alpha,\beta}(\mathbf{q})$ are related to the averaged electronic and spin densities on the xy plane by

$$n_\alpha(\mathbf{r}) = \frac{1}{2\pi\ell^2}\sum_{\mathbf{q}}\langle\rho_{\alpha,\alpha}(\mathbf{q})\rangle e^{-q^2\ell^2/4}e^{i\mathbf{q}\cdot\mathbf{r}}, \tag{6}$$

$$S_x(\mathbf{r}) = \frac{1}{2\pi\ell^2}\sum_{\mathbf{q}}\mathrm{Re}\left[\langle\rho_{+,-}(\mathbf{q})\rangle e^{-q^2\ell^2/4}e^{i\mathbf{q}\cdot\mathbf{r}}\right], \tag{7}$$

$$S_y(\mathbf{r}) = \frac{1}{2\pi\ell^2}\sum_{\mathbf{q}}\mathrm{Im}\left[\langle\rho_{+,-}(\mathbf{q})\rangle e^{-q^2\ell^2/4}e^{i\mathbf{q}\cdot\mathbf{r}}\right], \tag{8}$$

$$S_z(\mathbf{r}) = \frac{\hbar}{2}[n_+(\mathbf{r}) - n_-(\mathbf{r})]. \tag{9}$$

The $\langle\rho_{\alpha,\beta}(\mathbf{q})\rangle's$ can be considered as the order parameters of an ordered phase of the 2DEG.

The averaged Hartree-Fock ground-state energy per electron at $\nu = 1$ is given by

$$\begin{aligned}\frac{\langle H_{HF}\rangle}{N_e} &= -\frac{\Delta_Z}{2}\sum_{\alpha}\alpha\langle\rho_{\alpha,\alpha}(0)\rangle \\ &\quad -\frac{1}{S}\sum_{\mathbf{q}}\sum_{\alpha}V_e(-\mathbf{q})F(\mathbf{q})\langle\rho_{\alpha,\alpha}(\mathbf{q})\rangle \\ &\quad +\frac{1}{2}\sum_{\alpha,\beta}\sum_{\mathbf{q}\neq 0}H(\mathbf{q})\langle\rho_{\alpha,\alpha}(-\mathbf{q})\rangle\langle\rho_{\beta,\beta}(\mathbf{q})\rangle \\ &\quad -\frac{1}{2}\sum_{\alpha,\beta}\sum_{\mathbf{q}}X(\mathbf{q})|\langle\rho_{\alpha,\beta}(\mathbf{q})\rangle|^2. \end{aligned} \tag{10}$$

The order parameters $\langle\rho_{\alpha,\beta}(\mathbf{q})\rangle$ are computed by solving the Hartree-Fock equation for the single-particle Green's function $G_{\alpha,\beta}(\mathbf{q},\tau)$ which is defined by

$$\begin{aligned}G_{\alpha,\beta}(\mathbf{q},\tau) &= \frac{1}{N_\varphi}\sum_{X,X'}e^{-(i/2)q_x(X+X')} \\ &\quad \times\delta_{X,X'-q_y\ell^2}G_{\alpha,\beta}(X,X',\tau), \end{aligned} \tag{11}$$

where

$$G_{\alpha,\beta}(X,X',\tau) = -\langle T c_{X,\alpha}(\tau)c^{\dagger}_{X',\beta}(0)\rangle. \tag{12}$$

They are obtained with the relation,

$$\langle\rho_{\alpha,\beta}(\mathbf{q})\rangle = G_{\beta,\alpha}(\mathbf{q},\tau = 0^-). \tag{13}$$

The Hartree-Fock equation of motion for the Green's function $G_{\alpha,\beta}(\mathbf{q},i\omega_n)$ is given [25] by

$$\begin{aligned}&\left[i\omega_n - \frac{1}{\hbar}\left(\alpha\frac{\Delta_Z}{2}-\mu\right)\right]G_{\alpha,\beta}(\mathbf{q},i\omega_n) \\ &\quad = \delta_{\mathbf{q},0}\delta_{\alpha,\beta} - \frac{e}{\hbar S}\sum_{\mathbf{q}'}V_e(\mathbf{q}-\mathbf{q}')F(|\mathbf{q}-\mathbf{q}'|) \\ &\qquad \times\gamma_{\mathbf{q},\mathbf{q}'}G_{\alpha,\beta}(\mathbf{q}',i\omega_n) + \frac{1}{\hbar}\sum_{\mathbf{q}'\neq\mathbf{q}}U^H(\mathbf{q}-\mathbf{q}')\gamma_{\mathbf{q},\mathbf{q}'}G_{\alpha,\beta}(\mathbf{q}',i\omega_n) \\ &\qquad -\frac{1}{\hbar}\sum_{\mathbf{q}'}\sum_{\gamma}U^F_{\alpha,\gamma}(\mathbf{q}-\mathbf{q}')\gamma_{\mathbf{q},\mathbf{q}'}G_{\gamma,\beta}(\mathbf{q}',i\omega_n), \end{aligned} \tag{14}$$

where

$$\gamma_{\mathbf{q},\mathbf{q}'} = e^{-i(\mathbf{q}\times\mathbf{q}')\cdot\hat{\mathbf{z}}\ell^2/2}, \tag{15}$$

and ω_n are fermionic Matsubara frequencies, μ is the chemical potential, and we have defined the potentials,

$$U^H(\mathbf{q}) = \sum_{\alpha}H(\mathbf{q})\langle\rho_{\alpha,\alpha}(\mathbf{q})\rangle, \tag{16}$$

$$U^F_{\alpha,\beta}(\mathbf{q}) = X(\mathbf{q})\langle\rho_{\beta,\alpha}(\mathbf{q})\rangle. \tag{17}$$

These potentials depend on the order parameters $\langle\rho_{\alpha,\beta}(\mathbf{q})\rangle$ that are unknown. The equation of motion for $G_{\alpha,\beta}(\mathbf{q},i\omega_n)$ must thus be solved numerically [25] by using a seed for the order parameters and then iterate Eq. (14) until a convergent solution is found. In the present case, the square lattice structure is fixed by the external potential. We thus try different seeds corresponding to different possible spin textures and see if they lead to a converging solution. We compare the energy of the different solutions that we find and choose as the ground state the lowest-energy one. We then compute the dispersion relation of the collective modes of this solution to make sure that it is a stable solution. The order-parameter space is too big to ensure that the solution that we retain is the true ground state of the interacting Hamiltonian. Strictly speaking, the self-consistent Hartree-Fock approach allows us to find the lowest-energy state among a set of most likely candidates.

The density of states $g(\omega)$ is obtained from the single-particle Green's function by using the relation,

$$g(\omega) = -\frac{N_\varphi}{\pi}\sum_{\alpha}\mathrm{Im}[G_{\alpha,\alpha}(\mathbf{q}=0,\omega+i\delta)]. \tag{18}$$

To find the dispersion relation of the collective modes, we derive the equation of motion in the generalized random-phase approximation for the two-particle Green's function,

$$\begin{aligned}\chi_{\alpha,\beta,\gamma,\delta}(\mathbf{q},\mathbf{q}';\tau) &= -N_\varphi\langle T\rho_{\alpha,\beta}(\mathbf{q},\tau)\rho_{\gamma,\delta}(-\mathbf{q}',0)\rangle \\ &\quad + N_\varphi\langle\rho_{\alpha,\beta}(\mathbf{q})\rangle\langle\rho_{\gamma,\delta}(-\mathbf{q}')\rangle. \end{aligned} \tag{19}$$

This equation is

$$\begin{aligned}&\chi_{\alpha,\beta,\gamma,\delta}(\mathbf{q},\mathbf{q}';i\Omega_n) \\ &\quad = \chi^{(0)}_{\alpha,\beta,\gamma,\delta}(\mathbf{q},\mathbf{q}';i\Omega_n) \\ &\qquad +\frac{1}{\hbar}\sum_{\xi,\lambda}\sum_{\mathbf{q}''}\chi^{(0)}_{\alpha,\beta,\xi,\xi}(\mathbf{q},\mathbf{q}'';i\Omega_n)H(\mathbf{q}'')\chi_{\lambda,\lambda,\gamma,\delta}(\mathbf{q}'',\mathbf{q}';i\Omega_n) \\ &\qquad -\frac{1}{\hbar}\sum_{\xi,\lambda}\sum_{\mathbf{q}''}\chi^{(0)}_{\alpha,\beta,\xi,\lambda}(\mathbf{q},\mathbf{q}'';i\Omega_n)X(\mathbf{q}'')\chi_{\lambda,\xi,\gamma,\delta}(\mathbf{q}'',\mathbf{q}';i\Omega_n), \end{aligned} \tag{20}$$

where Ω_n is a bosonic Matsubara frequency. Equation (20) represents the summation of bubble (polarization effects) and ladder (excitonic corrections) diagrams. The Hartree-Fock two-particle Green's function (the single-bubble Feynman diagram with Hartree-Fock propagators) that enters this equation is obtained from the Hartree-Fock equation of motion for $\chi_{\alpha,\beta,\gamma,\delta}(\mathbf{q},\mathbf{q}';\tau)$ and is given by

$$\begin{aligned}&[i\hbar\Omega_n + (E_\alpha - E_\beta)]\chi^{(0)}_{\alpha,\beta,\gamma,\delta}(\mathbf{q},\mathbf{q}',i\Omega_n) \\ &\quad = \hbar[\gamma^*_{\mathbf{q},\mathbf{q}'}\langle\rho_{\alpha,\delta}(\mathbf{q}-\mathbf{q}')\rangle\delta_{\beta,\gamma} - \gamma_{\mathbf{q},\mathbf{q}'}\langle\rho_{\gamma,\beta}(\mathbf{q}-\mathbf{q}')\rangle\delta_{\alpha,\delta}] \\ &\qquad -\frac{e}{S}\sum_{\mathbf{q}''}V_e(\mathbf{q}-\mathbf{q}'')F(|\mathbf{q}-\mathbf{q}''|)[\gamma^*_{\mathbf{q},\mathbf{q}''} - \gamma_{\mathbf{q},\mathbf{q}''}] \\ &\qquad \times\chi^{(0)}_{\alpha,\beta,\gamma,\delta}(\mathbf{q}'',\mathbf{q}',i\Omega_n) \\ &\qquad -\sum_{\mathbf{q}''\neq 0}U^H(\mathbf{q}-\mathbf{q}'')[\gamma^*_{\mathbf{q},\mathbf{q}''}-\gamma_{\mathbf{q},\mathbf{q}''}]\chi^{(0)}_{\alpha,\beta,\gamma,\delta}(\mathbf{q}'',\mathbf{q}',i\Omega_n) \\ &\qquad +\sum_{\alpha'}\sum_{\mathbf{q}''}U^F_{\alpha,\alpha'}(\mathbf{q}-\mathbf{q}'')\gamma^*_{\mathbf{q},\mathbf{q}''}\chi^{(0)}_{\alpha',\beta,\gamma,\delta}(\mathbf{q}'',\mathbf{q}',i\Omega_n) \\ &\qquad -\sum_{\beta'}\sum_{\mathbf{q}''}U^F_{\beta',\beta}(\mathbf{q}-\mathbf{q}'')\gamma_{\mathbf{q},\mathbf{q}''}\chi^{(0)}_{\alpha,\beta',\gamma,\delta}(\mathbf{q}'',\mathbf{q}',i\Omega_n). \end{aligned} \tag{21}$$

By defining the superindices $I = (\alpha,\beta)$ and $J = (\gamma,\delta)$, Eq. (20) can be rewritten as a 4×4 matrix equation for the matrix of Green's functions $\chi_{I,J}$. This equation has

the form $[i\Omega_n I - F]\chi = B$. The matrix F, which depends only on the $\langle\rho_{\alpha,\beta}(\mathbf{q})\rangle$'s, is then diagonalized numerically to find $\chi_{I,J}$. The retarded response functions are obtained with the analytic continuation $i\Omega_n \to \omega + i\delta$. We compute the following density and spin responses:

$$\chi^R_{\rho_i,\rho_j}(\mathbf{q},\mathbf{q}';\omega) = -iN_\phi[\langle[\rho_i(\mathbf{q},t),\rho_j(-\mathbf{q}',t')]\rangle\theta(t-t')]_\omega, \tag{22}$$

where $i = n,x,y,z$ and the operators,

$$\rho_x = \tfrac{1}{2}[\rho_{+,-} + \rho_{-,+}], \tag{23}$$

$$\rho_x = \frac{1}{2i}[\rho_{+,-} - \rho_{-,+}], \tag{24}$$

$$\rho_z = \tfrac{1}{2}[\rho_{+,+} - \rho_{-,-}], \tag{25}$$

$$\rho_n = \rho_{+,+} + \rho_{-,-}. \tag{26}$$

In a uniform phase, the order parameters $\langle\rho_{\alpha,\beta}(\mathbf{q})\rangle$ are finite only when $\mathbf{q} = 0$, whereas in a two-dimensional CDW, they can be nonzero each time $\mathbf{q} = \mathbf{G}$, where $\mathbf{G}$ is a reciprocal lattice vector of the CDW. For the response function, we have to compute $\chi^R_{\rho_i,\rho_j}(\mathbf{q},\mathbf{q};\omega)$ in the uniform phase and $\chi^R_{\rho_i,\rho_j}(\mathbf{k}+\mathbf{G},\mathbf{k}+\mathbf{G}';\omega)$ in the CDW where $\mathbf{k}$ is by definition a vector in the first Brillouin zone of the CDW. In the CDW, the GRPA matrices F and B have dimensions of $4n_R \times 4n_R$, where n_R is the number of reciprocal lattice vectors considered in the numerical calculation. We typically take $n_R \approx 600$.

The formalism developed in this section can also be applied to the 2DEG in graphene if the electrons are assumed to occupy only one of the two valleys. In Landau-level $N = 0$ of graphene (and only in this level), the form factor $F(\mathbf{q})$ and the Hartree and Fock interactions $H(\mathbf{q})$ and $X(\mathbf{q})$ are the same as those given in Eqs. (2) and (4).

III. PHASE DIAGRAM FOR $\nu = 1$

We study the phase diagram of the 2DEG at filling factor $\nu = 1$ in Landau-level $N = 0$ and at a temperature of $T = 0$ K. For the external potential, we choose the simple square lattice form

$$V_e(\mathbf{r}) = 2V_e\left[\cos\left(\frac{2\pi}{\sqrt{2}a_0}(x+y)\right) + \cos\left(\frac{2\pi}{\sqrt{2}a_0}(x-y)\right)\right], \tag{27}$$

so that $V_e(\mathbf{q}) = SV_e\delta_{\mathbf{q},\mathbf{G}_1}$ in Eq. (1) with the vectors $\mathbf{G}_1 \in \frac{2\pi}{\sqrt{2}a_0}\{(1,1),(1,-1),(-1,1),(-1,-1)\}$. This external potential tries to impose a two-dimensional density modulation of the 2DEG with a square lattice constant a_0. We allow the spin texture (if any) to have the bigger lattice constant $\sqrt{2}a_0$ by considering the order parameters $\langle\rho_{\alpha,\beta}(\mathbf{G})\rangle$ with reciprocal lattice vectors given by $\mathbf{G} = \frac{2\pi}{\sqrt{2}a_0}(n,m)$, where $n,m = 0, \pm 1, \pm 2, \ldots$. The *density* unit cell has a lattice constant a_0 whereas the *magnetic* unit cell has a lattice constant $\sqrt{2}a_0$. For the potential strength, we use $W_0 = eV_eF(G_1)$ [see Eq. (14)], where $G_1 = 2\pi/a_0$. The critical values of W_0 (not V_e) for the transition between the uniform and the modulated phases at different values of Γ are similar. Hereafter, we give all energies in units of $e^2/\kappa\ell$. We make the important assumption that Landau-level mixing by both the Coulomb interaction and the external potential can be neglected, i.e., we work in the limit of a weak superlattice potential. We also neglect disorder effect and work at zero temperature.

The ratio ℓ/a_0 that enters the Hartree-Fock energy and the equation of motion for the single-particle Green's function is given by

$$\frac{\ell}{a_0} = \sqrt{\frac{1}{2\pi}\frac{\varphi_0}{Ba_0^2}} \equiv \sqrt{\frac{\Gamma}{2\pi}}, \tag{28}$$

where $\varphi_0 = hc/e$ is the flux quantum. The important parameter Γ^{-1} is the number of flux quanta piercing a *density* unit-cell area. With this definition, the factor $F(G_1) = e^{-G_1^2\ell^2/4} = e^{-\pi\Gamma}$. We limit our analysis to $\Gamma = q/p$ where q and p are integers with no common factors.

In Landau-level $N = 0$, a Wigner crystal [2] with a triangular lattice can form at sufficiently small filling factor ν [26]. At $\nu = 1$, however, the ground state of the 2DEG is a uniform electron liquid with full spin polarization, i.e., a quantum Hall ferromagnet [27] (QHF) whose energy per electron is given by

$$\frac{\langle H_{HF}\rangle}{N_e} = -\frac{\Delta_Z}{2} - \frac{1}{2}\sqrt{\frac{\pi}{2}}\left(\frac{e^2}{\kappa\ell}\right) \tag{29}$$

(neglecting the kinetic energy that is a constant in $N = 0$). The QHF remains the ground state even when the Zeeman coupling goes to zero because a perfect alignment of the spins minimizes the Coulomb exchange energy [the second term on the right-hand side of Eq. (29)]. In a uniform state, the Coulomb-Hartree energy is canceled by the neutralizing uniform positive background.

A. Case of $\Gamma \in [1/2,1]$

We first consider the case of $\Gamma \in [1/2,1]$. Figure 1 shows the ground-state energy and spin-polarization $S_z/\hbar$ as a function of the potential W_0 for $\Gamma = 1/2,2/3,3/4,4/5,1$ and for a Zeeman coupling $\Delta_Z = 0.015$. The ground state is spatially uniform and has an energy $\langle H_{HF}\rangle$ and a spin-polarization S_z that remain constant until a critical field $W_0^{(c)} \approx 0.11$. This uniform state is described by only one order parameter, i.e., $\langle\rho_{+,+}(0)\rangle = 1$ and is fully spin polarized, i.e., the spin per electron is $S_z = \hbar/2$. The corresponding change in the density of states (DOS) with W_0 is shown in Fig. 2. In the absence of an external potential and a Coulomb interaction, the DOS has two peaks at energies $E_\pm = \pm\Delta_Z/2$ corresponding to the two spin states. With the Coulomb interaction, the Zeeman gap Δ_Z is strongly renormalized [see Fig. 2(a)] as is well known. When the external potential is present, the DOS for each spin orientation has p peaks corresponding to the number of sub-bands expected when an electron is submitted to both a magnetic field and a weak periodic potential [14]. This is clearly visible in Figs. 2(a), 2(d), and 2(e) for $\Gamma = 1,2/3,4/5$. The external potential increases the width of the peaks in the DOS and decreases the renormalized Zeeman gap (which is also the transport gap). We remark that the rapid oscillations in some of the graphs at $\Gamma = 1$ are a numerical artifact. They

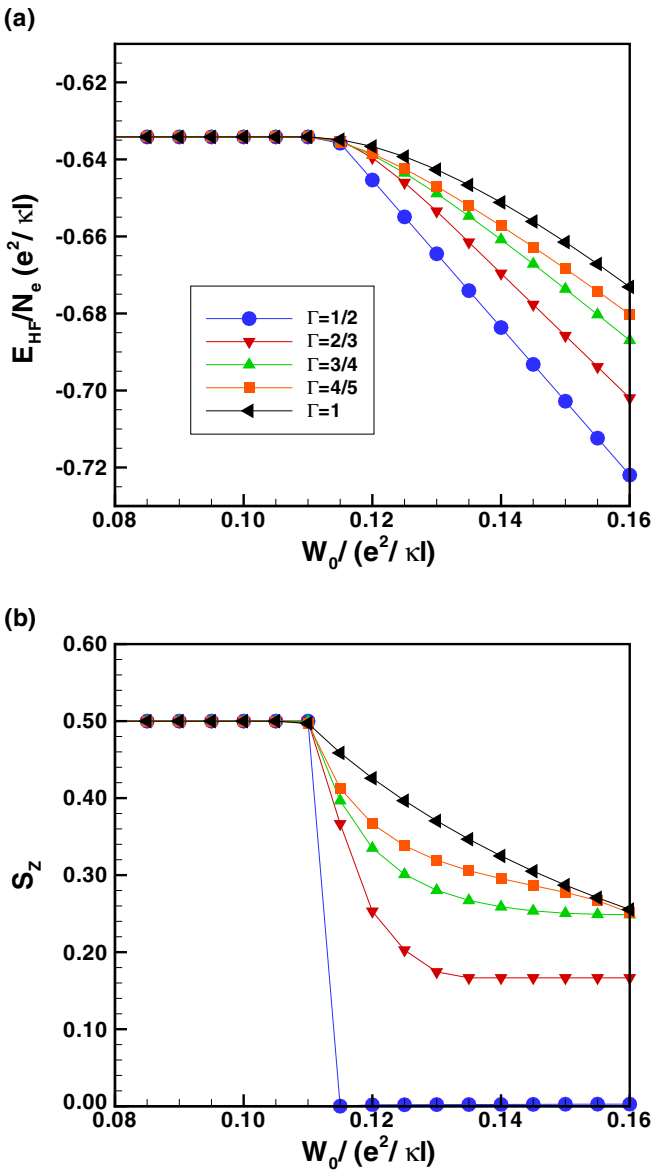

FIG. 1. (a) Hartree-Fock energy per electron and (b) average spin per electron $S_z/\hbar$ as a function of the applied external field W_0 for different values of Γ at filling factor $\nu = 1$ in Landau-level $N = 0$ and for the Zeeman coupling $\Delta_Z/(e^2/\kappa\ell) = 0.015$.

depend strongly on the number of reciprocal lattice vectors kept in the calculation.

If we enforce the uniform solution beyond the critical value of $W_0^{(c)} \approx 0.11$, we find that the transport gap closes at $W_0 \approx 0.15$ for $\Gamma = 1$ where the system becomes metallic. Our code no longer converges in this case. But this transition to a metallic state does not occur because the uniform state becomes unstable at $W_0^{(c)}$. The stability of a state is evaluated by computing the dispersion relation of its collective modes. For the uniform state, the collective excitations reduce to a spin-wave mode. When $W_0 = 0$, the spin-wave dispersion is given by [28]

$$\omega_{SW}(\mathbf{k}) = \Delta_Z + \left(\frac{e^2}{\kappa\ell}\right)[X(0) - X(\mathbf{k})]. \qquad (30)$$

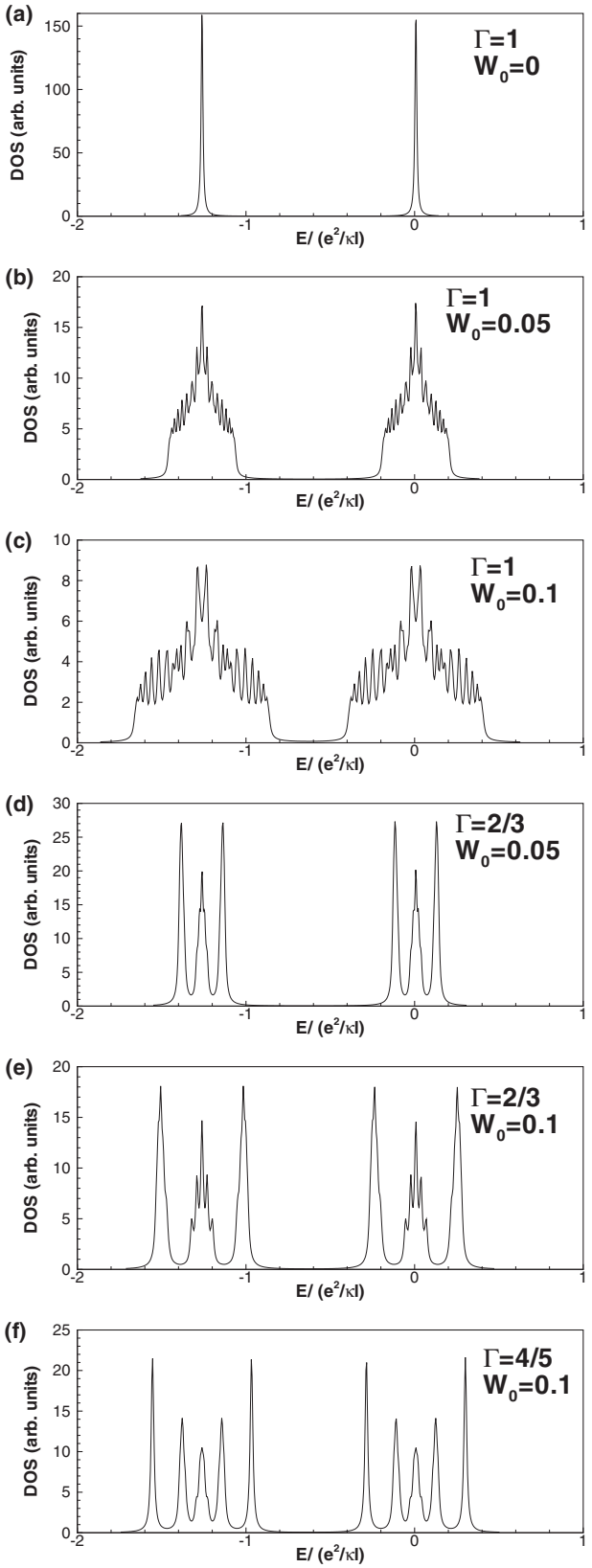

FIG. 2. Density of states for the uniform fully spin-polarized phase at $\nu = 1$ in Landau-level $N = 0$ for Zeeman coupling $\Delta_Z = 0.015$. (a)–(c) $\Gamma = 1$ and $W_0 = 0, 0.05, 0.1$, respectively; (d) and (e) $\Gamma = 2/3$ and $W_0 = 0.05, 0.1$, respectively; (f) $\Gamma = 4/5$ and $W_0 = 0.1$. The rapid oscillations in some of the graphs are a numerical artifact. All energies are in units of $e^2/\kappa\ell$.

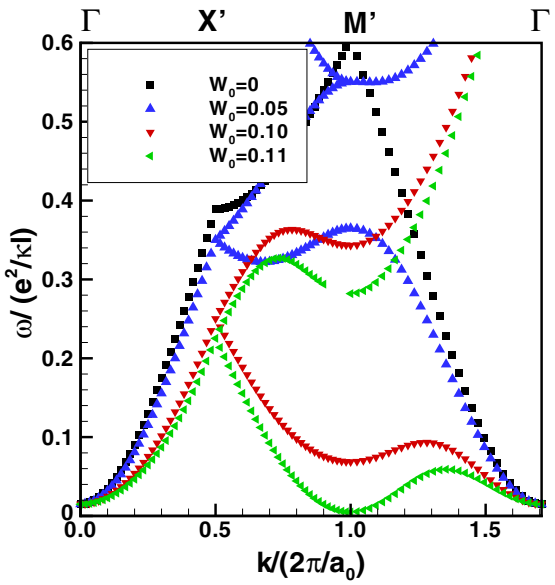

FIG. 3. Dispersion relation of the spin-wave mode in the uniform fully spin-polarized state at $\nu = 1$, $N = 0$ for $\Gamma = 1$, $\Delta_Z = 0.015$ and different values of the external potential W_0. The wave-vector $\mathbf{k}$ follows the path $\Gamma - X' - M' - \Gamma$ along the irreducible (density) Brillouin zone of the square lattice. All energies are in units of $e^2/\kappa\ell$.

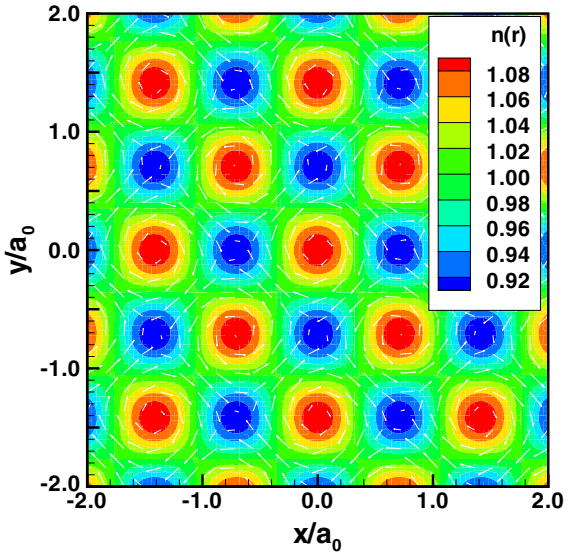

FIG. 4. Vortex-CDW phase of the 2DEG at $\nu = 1$ in Landau-level $N = 0$ for $W_0 = 0.12$ and Zeeman coupling $\Delta_Z = 0.015$. The electronic density $n(\mathbf{r})$ is in units of $(2\pi\ell^2)^{-1}$. The vector field shows the vortex structure on the xy plane for the parallel component of the spin vector. All energies are in units of $e^2/\kappa\ell$.

This mode is gapped at the bare Zeeman energy and saturates at $\omega_{SW}(\mathbf{k}\to\infty) = \Delta_Z + \sqrt{\frac{\pi}{2}}(\frac{e^2}{\kappa\ell})$. Figure 3 shows its dispersion for $\Gamma = 1$ and $W_0 = 0,0.05,0.10,0.11$. The wave-vector $\mathbf{k}$ runs along the path $\Gamma - X' - M' - \Gamma$, i.e., along the edges of the irreducible *density* Brillouin zone [with $\Gamma = (0,0)$, $M' = (1/\sqrt{2},0)$, $X' = (1/2\sqrt{2},1/2\sqrt{2})$ in units of $2\pi/a_0$]. The spin-wave mode softens at a finite wave-vector $\mathbf{k}$ as W_0 increases so that the uniform state becomes unstable at $W_0^{(c)} \approx 0.11$, which is also the value at which the 2DEG is seen to enter a new phase in Fig. 1(a). When plotted in the reduced zone scheme as in Fig. 3, the spin-wave mode is split into several branches that accumulate into a very dense manifold near $\omega_{SW}(\mathbf{k}\to\infty)$. Only some of these branches are shown in Fig. 3 since we are interested only in the low-energy sector. The spin-wave dispersion is obtained by following the pole of the response functions $\chi^R_{\rho_+,\rho_-}(\mathbf{k},\mathbf{k};\omega t)$ with $\rho_\pm = \rho_x \pm i\rho_y$ for different values of $\mathbf{k}$. We remark that the softening of the spin-wave mode by a *one-dimensional* external potential was reported previously by Bychkov *et al.* [29]. These authors suggested that the resulting condensation of the spin excitons at the softening wave vector would create a new spin-density-wave ground state. This is precisely what we find but this time for a *two-dimensional* surface potential.

The ground state in a small region of W_0 after $W_0^{(c)}$ is a charge density wave with a vortex spin texture. Hereafter, we refer to this state as the vortex CDW. The range of W_0 where the vortex CDW is the ground state depends on Γ and Δ_Z. The electronic density and spin texture of the vortex CDW are shown in Fig. 4 for the parameters $\Gamma = 1$ and $W_0 = 0.12$, $\Delta_Z = 0.015$. The value of $W_0 = 0.12$ is close to $W_0^{(c)}$ so that the amplitude of the CDW in this figure is small. The amplitude increases with W_0 however. Minima and maxima of the CDW have the same amplitude, and there is no net-induced charge in a unit cell as expected. The spin-density $S_z(\mathbf{r})$ (not shown in the figure) varies only slightly.

The spin texture of the vortex CDW is interesting. There is a 2π spin vortex at each positive and negative modulation of the density. Since the z component of the spin is everywhere positive and because of the spin-charge coupling inherent to a QHF [27], the positive and negative modulations have opposite vorticities. We could, loosely speaking, refer to the positive and negative modulations as merons and antimerons. A meron is an excitation of a unit vector field $\mathbf{m}(\mathbf{r})$ that has $m_z(0) = \pm 1$ at its center and $m_z(\mathbf{r}) = 0$ far away from the center where the vectors lie on the xy plane and form a vortex configuration with vorticity $n_v = \pm 1$. As r increases from the meron core, the spins smoothly rotate up [if $m_z(0) = -1$] or down [if $m_z(0) = +1$] towards the xy plane. There are four flavors of merons [27] with a topological charge given by $Q = \frac{1}{2}[m_z(\infty) - m_z(0)]n_v$. In a QHF, merons carry half an electron charge. In our vortex CDW however, we are dealing with a spin-density $\mathbf{S}(\mathbf{r})$ that does not have $|\mathbf{S}(\mathbf{r})| = \hbar/2$ everywhere in space (the vectors do not just rotate) so that our merons do not have a quantized charge. But, for a given sign of $S_z(0)$ the meron and antimeron have opposite vorticities and so opposite electrical charges. Moreover, our merons are closely packed in a square lattice and have a large core so that the spin vector tilts towards the xy plane but $S_z(0)$ does not go to zero between two adjacent merons.

In each magnetic unit cell of the vortex CDW, there are two merons and two antimerons with the same vorticity but opposite global phase for two merons or antimerons. This bipartite meron lattice is similar to the square lattice antiferromagnetic state of the Skyrme crystal that was predicted to occur in a 2DEG near (but not at) filling factor $\nu = 1$ in the absence of an external potential [22]. In the Skyrme crystal, the electrons (or holes) added to the QHF state at $\nu = 1$ crystallize in the

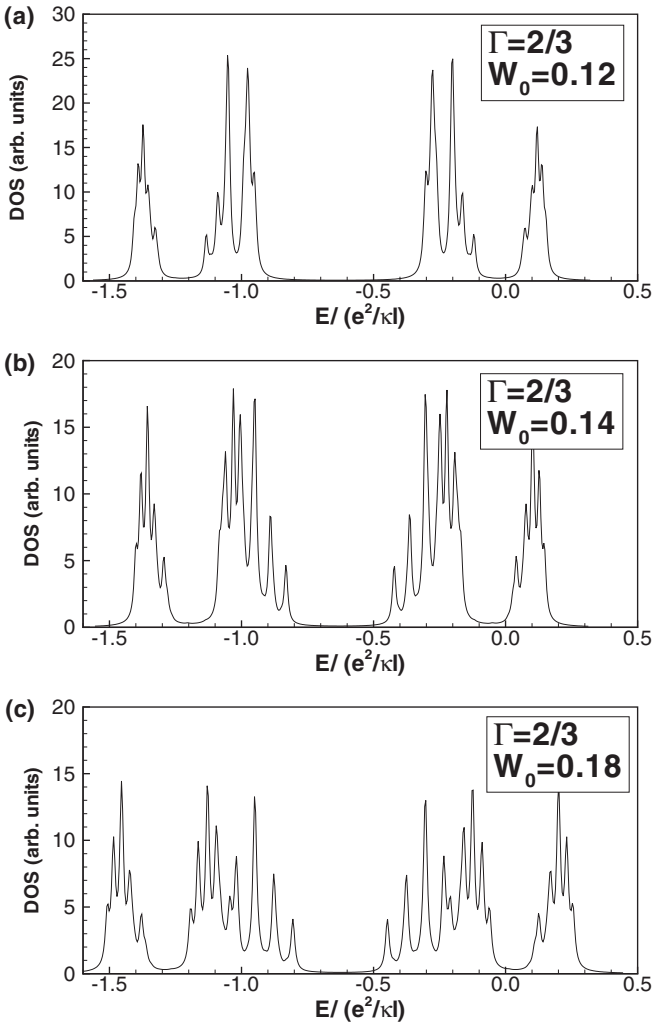

FIG. 5. Density of states in the vortex CDW at $\nu = 1$ in Landau-level $N = 0$ for $\Gamma = 2/3$, Zeeman coupling $\Delta_Z = 0.015$, and different values of W_0 (all energies are in units of $e^2/\kappa\ell$).

form of skyrmions for $\nu > 1$ or antiskyrmions for $\nu < 1$. The vortex CDW that we find here occurs *at* precisely $\nu = 1$.

Figure 1(b) shows that the average spin S_z decreases with W_0 in the vortex CDW and saturates at the precise value of $S_z = \Gamma - 1/2$ for $\Gamma = 1/2,2/3,3/4$. In the saturation region for S_z, the spin texture has disappeared, and the CDW has very little modulation in $S_z(\mathbf{r})$. We will call this phase the normal CDW. There is no saturation for the two cases of $\Gamma = 4/5,1$. The GRPA indicates that the meron CDW becomes unstable above $W_0 \approx 0.16$ for $\Gamma = 4/5,1$ but none of the seeds that we have tried lead to a stable solution. We thus limit our analysis to the range of $W_0 \in [0,0.16]$ for most values of Γ in this paper. More work is needed to establish the phase diagram at larger values of W_0. The change in S_z induced by the external potential should be detectable experimentally. In particular, the vortex CDW is absent for $\Gamma = 1/2$, and thus the 2DEG makes a transition from a fully polarized to an unpolarized CDW with period a_0 instead of $\sqrt{2}a_0$.

The density of states for the vortex CDW is shown in Fig. 5 for $\Gamma = 2/3$ and $W_0 = 0.12,0.14,0.18$. The sub-band structure gets more and more different from that of the uniform phase

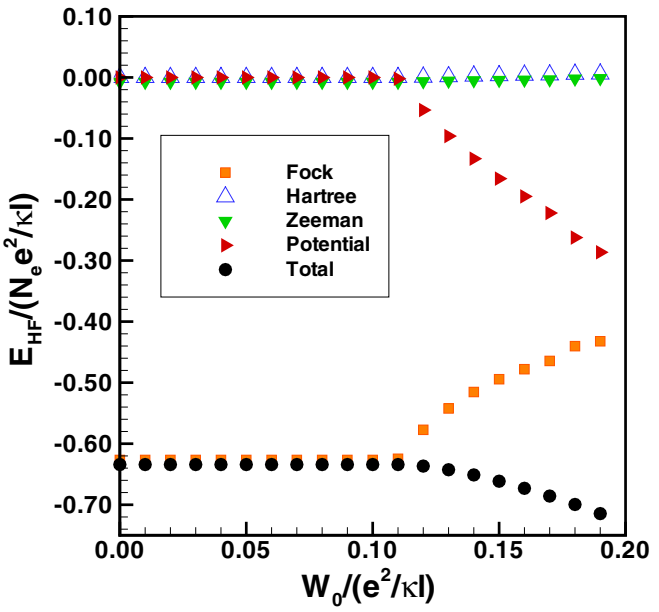

FIG. 6. Behavior with W_0 of different contributions to the total energy of the uniform and vortex-CDW states for $\Gamma = 1$ and the Zeeman coupling $\Delta_Z = 0.015$.

as W_0 increases [compare with Fig. 2(e)]. The electron-hole gap decreases slowly with W_0 in the vortex-CDW and normal-CDW phases.

Figure 6 shows the Hartree, Fock (or exchange), external potential, and Zeeman contributions to the total energy of the vortex CDW and uniform state for $\Gamma = 1$ and Zeeman coupling $\Delta_Z = 0.015$. The Hartree energy is zero in the uniform phase and small in the vortex-CDW phase. The Zeeman energy is also very small in both phases. The competition is between the Fock and the external potential energies. The former is minimal in the uniform state and increases with W_0 in the vortex-CDW phase. The latter is zero in the uniform phase but decreases with W_0 in the vortex-CDW state. Figure 6 shows that the increase in exchange energy is more than compensated by the decrease in the external potential energy when the vortex CDW is formed.

The energy of the vortex-CDW state does not depend on the global phase of its vortices. This $U(1)$ symmetry, which is broken in a particular realization of the vortex-CDW state, leads to a gapless phase mode (a Goldstone mode). This is clearly seen in Fig. 7(b) where the two modes for $\omega < 0.05e^2/\hbar\kappa\ell$ are the spin-wave mode which is gapped at Δ_Z and the gapless phase mode. In Fig. 7, $\Gamma = 2/3$, and the wave-vector $\mathbf{k}$ now follows the path $\Gamma - M - X - \Gamma$ along the edges of the irreducible *magnetic* Brillouin zone of the square lattice [with $\Gamma = (0,0)$, $M = (1/2\sqrt{2},1/2\sqrt{2})$, $X = (1/2\sqrt{2},0)$ in units of $2\pi/a_0$]. To obtain the dispersions in the CDW phases, we have computed the response functions $\sum_{\mathbf{G}} \chi^R_{\rho_j,\rho_j}(\mathbf{k}+\mathbf{G},\mathbf{k}+\mathbf{G},\omega)$ with $j = n,x,y,z$ keeping the first 25 reciprocal lattice vectors in the summation. The summation allows the capture of modes that originate from a folding of the full dispersion into the first Brillouin zone. It also captures the electron-hole continuum [30] that starts at the Hartree-Fock gap. In Fig. 7, we have cut the dispersions

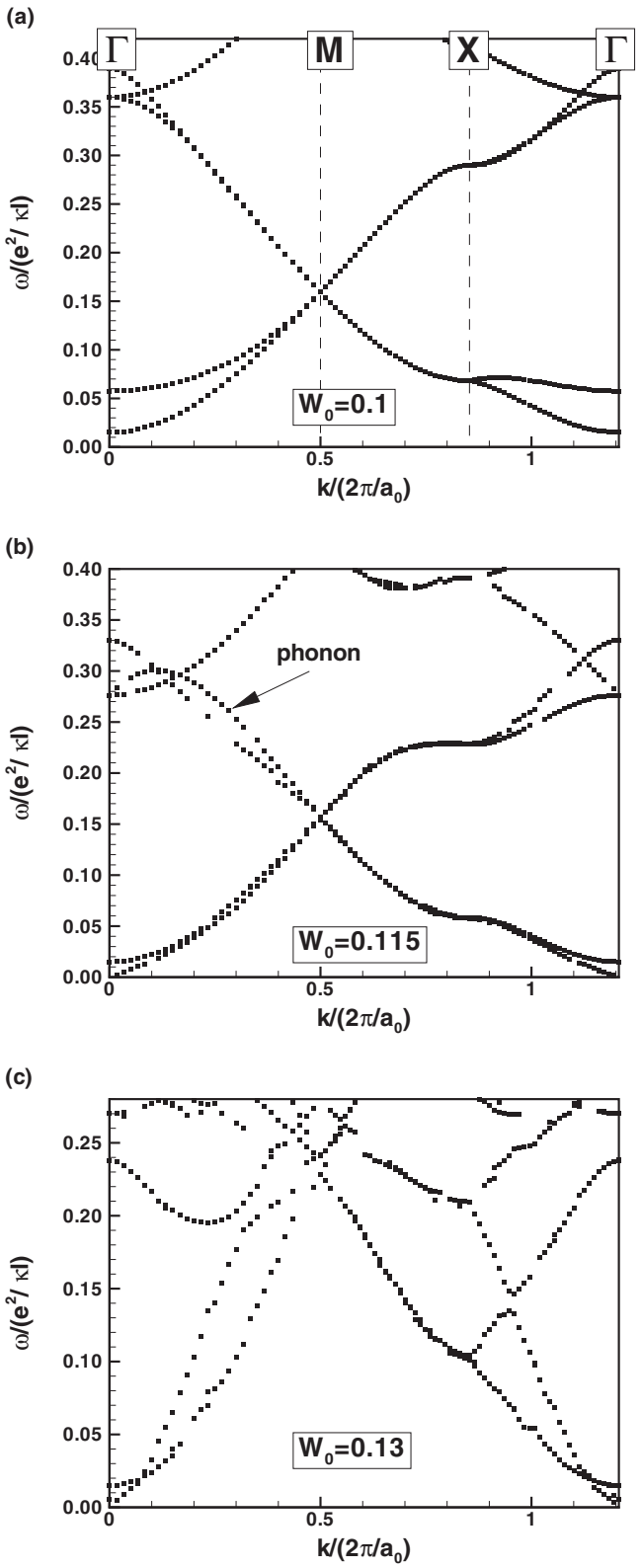

FIG. 7. Dispersion relations of the collective modes at $\nu = 1$ in Landau-level $N = 0$ for $\Gamma = 2/3$ and Zeeman coupling $\Delta_Z = 0.015$. (a) $W_0 = 0.1$; (b) $W = 0.115$; and (c) $W = 0.13$. All energies are in units of $e^2/\kappa\ell$.

at a frequency corresponding to the onset of this continuum. Figure 7 shows the dispersion for: (a) the uniform phase, (b) the vortex CDW, and (c) the normal CDW.

The vortex and normal CDWs have phonon modes gapped by the external potential. The branch we indicate as the gapped phonon mode in Fig. 7(b) has the strongest peak in the response function $\chi^R_{\rho_n,\rho_n}(\mathbf{k},\mathbf{k},\omega)$ (no summation over $\mathbf{G}$) as $\mathbf{k} \to 0$ whereas the spin-wave and phase modes are stronger in $\chi^R_{\rho_+,\rho_-}(\mathbf{k},\mathbf{k},\omega)$ and $\chi^R_{\rho_z,\rho_z}(\mathbf{k},\mathbf{k},\omega)$, respectively. At $W_0 = 0.13$ for $\Gamma = 2/3$, the ground state has transited to the normal CDW, and the phase mode is gapped as shown in Fig. 7(c).

B. Case of $\Gamma \in [0,1/2]$

The phase diagram for $\Gamma \in [0,1/2]$ is different from that of $\Gamma \in [1/2,1]$. For $\Gamma \in [0,1/2]$, we find a transition between two types of vortex-CDW phases. The first vortex CDW is the one described in the previous section; the second one, the antivortex CDW, has the sign of all vortices and S_z inverted (but different amplitudes for the charge and spin modulations). This antivortex CDW evolves from a uniform state that has all spins down as shown in Fig. 8. At $\Delta_Z = 0$, these two CDWs are degenerate in energy. At finite Zeeman coupling, there is a crossing between the energy curves of these two phases. The ground state thus evolves from the uniform state with all spins up to the vortex CDW, then to the antivortex CDW, and finally into the normal CDW. Figure 8 shows these transitions for the special cases of $\Gamma = 1/3$ and $\Delta_Z = 0.015, 0.006, 0.002$. The corresponding behavior of S_z is also shown. The region where S_z varies in each graph is where the vortex (or antivortex) CDW is the ground state. As the Zeeman coupling gets smaller, this region increases. The value of W_0 for the crossing between the two vortex-CDW states is shown by the dashed vertical line in the S_z vs W_0 curves. The average spin S_z changes discontinuously at this point, but this discontinuity goes to zero as $\Delta_Z \to 0$. The value of S_z is always positive, however. For $\Gamma \in [1/2,1]$, the energy curve for the antivortex CDW is above that of the vortex CDW for all values of W_0. The two curves merge at $\Delta_Z = 0$, but there is no crossing between the two solutions. If we take advantage of the possibility of changing the value of the g factor independently of the magnetic field in GaAs/AlGaAs heterojunctions, then it is possible to reduce the Zeeman coupling and as Fig. 9 clearly shows to increase the transition region where the vortex CDW is expected.

Figure 9 shows the behavior of S_z in the ground state for $\Gamma = 1/2, 1/3, 1/4, 1/5$ and a very small Zeeman coupling $\Delta_Z = 0.001$. The vertical dashed lines indicate where the transition between the vortex- and antivortex-CDW phases occurs for each value of Γ. The spin starts at $S_z/\hbar = 1/2$ in the uniform state then decreases in the vortex CDW (open symbols in Fig. 9). When the antivortex CDW replaces the vortex CDW as the ground state of the system, the value of S_z changes discontinuously. This jump is more apparent for $\Gamma = 1/5$ in Fig. 9. After this discontinuity, S_z increases (filled symbols in Fig. 9) until it reaches the finite value of $S_z/\hbar = \frac{1}{2} - \Gamma$ at large W_0, a value that is independent of the Zeeman coupling Δ_Z. The behavior of S_z is not monotonous. In the limit $\Delta_Z \to 0$, the S_z curves for the vortex and antivortex CDWs would cross at $S_z = 0$, and there would be no discontinuity. In the special case of $\Gamma = 1/2$, the transition is directly from the uniform and fully polarized state with $S_z/\hbar = 1/2$ to the normal CDW where $S_z = 0$. There is thus an important discontinuity in S_z in this case.

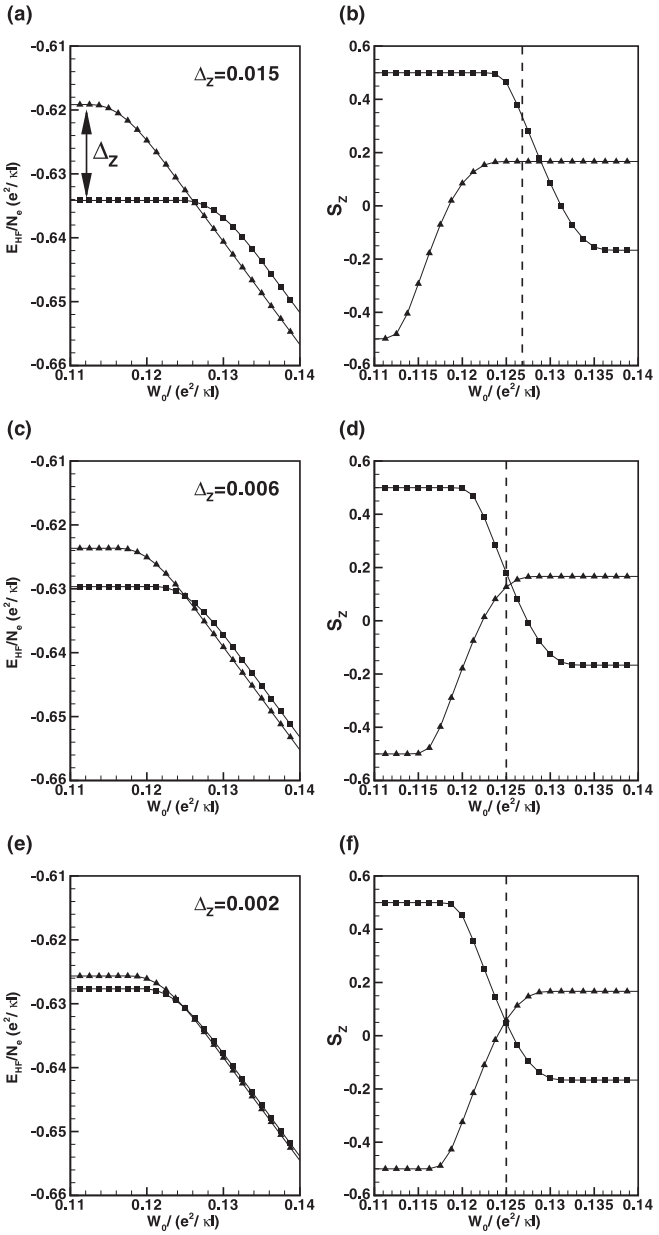

FIG. 8. Energy (left) and corresponding average spin $S_z/\hbar$ per electron (right) of the vortex CDW (squares) and antivortex CDW (triangles) for $\Gamma = 1/3$ and Zeeman couplings: (a) and (b) $\Delta_Z = 0.015$; (c) and (d) $\Delta_Z = 0.006$; (e) and (f) $\Delta_Z = 0.002$ in units of $e^2/\kappa\ell$. The vertical dashed lines indicate the value of the potential W_0 at which the transition between the two vortex CDWs takes place.

As we mentioned above, our formalism can equally well be used to discuss the energy of the electron gas in Landau-level $N = 0$ in graphene if the electrons are assumed to occupy only one valley. An exact diagonalization study by Ghazaryan and Chakraborty [31] for a 2DEG in graphene finds transition between unpolarized and partially polarized ground states induced by the external potential when $\Gamma = 1$ (their $\alpha = 1$). Equation (14) was also used [32] to study the effect of the Coulomb interaction on the density of states for graphene in a modulated potential but the vortex-CDW state that we found was not considered in that work.

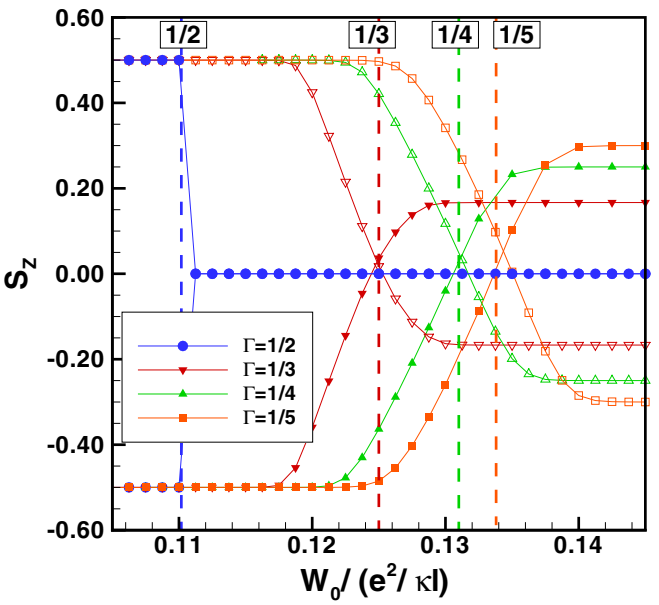

FIG. 9. Spin-polarization $S_z/\hbar$ as a function of the applied external potential W_0 for several values of $\Gamma \leqslant 1/2$ and Zeeman coupling $\Delta_Z = 0.001e^2/\kappa\ell$. The vertical dashed lines indicate the potential strength W_0 for each value of Γ where the transition from the vortex (filled symbols) to the antivortex CDW (open symbols) takes place. For $\Gamma = 1/2$, the transition is from the uniform (with $S_z/\hbar = 1/2M$) to the normal CDW with $S_z = 0$.

IV. SUMMARY AND DISCUSSION

We have computed the phase diagram of the 2DEG at $\nu = 1$ in Landau-level $N = 0$ in the presence of an applied external potential with a square lattice periodicity for several rational values of $\Gamma \in [0,1]$. We restricted our analysis to $W_0 \in [0,0.16]$. In this range, the 2DEG evolves first from a uniform state with full spin polarization, then to a vortex-CDW state and (if $\Gamma < 1/2$) antivortex-CDW state, and finally into a normal CDW with no spin texture but with a finite spin-polarization S_z if $\Gamma \neq 1/2$.

The change in the spin-polarization S_z with the applied field (smooth for $\Gamma > 1/2$ and abrupt for $\Gamma \leqslant 1/2$) is one feature of the phase transition described in this paper that should be measurable experimentally. Another one is the gapless spin mode due to the broken $U(1)$ symmetry in the vortex-CDW phase. The same mode occurs in a Skyrme crystal. In that system, it was shown that such a mode could provide a fast channel for the relaxation of the nuclear spin in nuclear magnetic resonance experiments [23]. Indeed, the bare Zeeman gap in the dispersion of the spin-wave mode is orders of magnitude larger than the nuclear spin splitting, impeding the creation of spin waves by nuclear spins. The softening of the spin-wave mode in the uniform phase may also lead to an increase in nuclear spin-lattice relaxation time as suggested by Bychkov *et al.* [29].

We have used W_0 for the external potential because the transition from the uniform to the vortex CDW takes place at roughly the same value of W_0 when the potential is expressed in terms of W_0. The actual external potential however is $V_e = F^{-1}(G_1)W_0 = e^{\pi\Gamma}W_0$. This means that the critical field

$W_0^{(c)} \approx 0.11$ translates into different real critical fields for different values of Γ, i.e., from $V_e^{(c)} = 0.21$ for $\Gamma = 1/5$ to $V_e^{(c)} = 2.5$ for $\Gamma = 1$. It is not clear then if our assumption of neglecting Landau-level mixing can be justified for Γ near unity. We assumed that the external lattice parameter a_0 is fixed experimentally. When Γ is also given, all other parameters are determined: the magnetic field, the electronic density n_e (at $\nu = 1$), and the ratio α of the Coulomb interaction to the cyclotron energy,

$$B = \frac{hc}{ea_0^2}\frac{1}{\Gamma} = \frac{4135.7}{\overline{a}_0^2}\frac{1}{\Gamma}\ \mathrm{T}, \tag{31}$$

$$n_e = \frac{1}{\Gamma a_0^2} = \frac{1}{\overline{a}_0^2}\frac{1}{\Gamma} \times 10^{14}\ \mathrm{cm}^{-2}, \tag{32}$$

$$\alpha = \frac{\frac{e^2}{\kappa\ell}}{\hbar\omega_c^*} = \frac{a_0}{a_{B^*}}\sqrt{\frac{\Gamma}{2\pi}} = \frac{\overline{a}_0}{10.2}\sqrt{\frac{\Gamma}{2\pi}}, \tag{33}$$

where $a_B^* = \kappa\hbar^2/m^*e^2$ is the effective Bohr radius and $\overline{a}_0$ is the lateral superlattice constant in nanometers. We used for GaAs $\kappa = 12.9$ and $m^* = 0.067m_e$ (where m_e is the electron mass).

For $\Gamma = 1$, $\alpha = 0.039\overline{a}_0$ so that with a very small (but physically feasible [16]) superlattice period of $a_0 = 39$ nm, we get $\alpha = 1.5$, $B = 2.7$ T, $n_e = 0.65 \times 10^{11}$ cm^{-2} whereas for $\Gamma = 1/5$, we get $\alpha = 0.68$, $B = 13.6$ T, $n_e = 3.29 \times 10^{11}$ cm^{-2}. The magnetic field and density pose no problem, but α is not small, especially when $\Gamma > 1/2$. Clearly, a more sophisticated calculation including a certain amount of Landau-level mixing and screening is required to confirm that the vortex-CDW phase is effectively the ground state in this system. We leave this for further work.

ACKNOWLEDGMENTS

R.C. was supported by a grant from the Natural Sciences and Engineering Research Council of Canada (NSERC). Computer time was provided by Calcul Québec and Compute Canada.

[1] For a review, see *The Quantum Hall Effect*, edited by R. E. Prange and S. M. Girvin (Springer-Verlag, New York, 1990); M. O. Goerbig, in *Ultracold Gases and Quantum Information, Lecture Notes of the Les Houches Summer School in Singapore, July 2009*, Vol. 91 (Oxford, 2011).

[2] E. P. Wigner, Phys. Rev. **46**, 1002 (1934).

[3] For reviews, see *Physics of the Electron Solid*, edited by S. T. Chui (International, Boston, 1994); H. Fertig and H. Shayegan, in *Perspectives in Quantum Hall Effects*, edited by S. Das Sarma and A. Pinczuk (Wiley, New York, 1997), Chaps. 3 and 9, respectively.

[4] For a review, see M. M. Fogler, in *High Magnetic Fields: Applications in Condensed Matter Physics and Spectroscopy*, edited by C. Berthier, L.-P. Levy, and G. Martinez (Springer-Verlag, Berlin, 2002), Chap. 4, pp. 98–138.

[5] S. L. Sondhi, A. Karlhede, S. A. Kivelson, and E. H. Rezayi, Phys. Rev. B **47**, 16419 (1993).

[6] For a review on skyrmions, see Z. F. Ezawa, *Quantum Hall Effects* (World Scientific, Singapore, 2000).

[7] S. M. Girvin and A. H. MacDonald in *Perspectives in Quantum Hall Effects*, edited by S. Das Sarma and A. Pinczuk (Wiley, New York, 1997), Chap. 5.

[8] For an early review of this problem, see, for example, D. Pfannkuche and R. R. Gerhardts, Phys. Rev. B **46**, 12606 (1992).

[9] A. Rauh, Phys. Status Solidi B **65**, K131 (1974); **69**, K9 (1975).

[10] R. R. Gerhardts, D. Weiss, and K. v. Klitzing, Phys. Rev. Lett. **62**, 1173 (1989); R. W. Winkler, J. P. Kotthaus, and K. Ploog, *ibid.* **62**, 1177 (1989); V. Gudmundsson and R. R. Gerhardts, Phys. Rev. B **52**, 16744 (1995).

[11] See, for example, T. Schlösser, K. Ensslin, J. P. Kotthaus, and M. Holland, Semicond. Sci. Technol. **11**, 1582 (1996), and references therein.

[12] D. J. Thouless, in *The Quantum Hall Effect*, edited by R. E. Prange and S. M. Girvin, Graduate Texts in Contemporary Physics (Springer-Verlag, New York, 1987), p. 101; M. C. Geisler, J. H. Smet, V. Umansky, K. von Klitzing, B. Naundorf, R. Ketzmerick, and H. Schweizer, Phys. Rev. Lett. **92**, 256801 (2004).

[13] G. Gumbs and P. Fekete, Phys. Rev. B **56**, 3787 (1997).

[14] D. R. Hofstadter, Phys. Rev. B **14**, 2239 (1976).

[15] C. Albrecht, J. H. Smet, K. von Klitzing, D. Weiss, V. Umansky, and H. Schweizer, Phys. Rev. Lett. **86**, 147 (2001).

[16] S. Melinte, M. Berciu, C. Zhou, E. Tutuc, S. J. Papadakis, C. Harrison, E. P. De Poortere, M. Wu, P. M. Chaikin, M. Shayegan, R. N. Bhatt, and R. A. Register, Phys. Rev. Lett. **92**, 036802 (2004).

[17] T. Schloesser, K. Ensslin, J. P. Kotthaus, and M. Holland, Europhys. Lett. **33**, 683 (1996); R. R. Gerhardts, D. Weiss, and U. Wulf, Phys. Rev. B **43**, 5192 (1991).

[18] C. R. Dean, L. Wang, P. Maher, C. Forsythe, F. Ghahari, Y. Gao, J. Katoch, M. Ishigami, P. Moon, M. Koshino, T. Taniguchi, K. Watanabe, K. L. Shepard, J. Hone, and P. Kim, Nature (London) **497**, 598 (2013).

[19] B. Hunt, J. D. Sanchez-Yamagishi, A. F. Young, M. Yankowitz, B. J. LeRoy, K. Watanabe, T. Taniguchi, P. Moon, M. Koshino, P. Jarillo-Herrero, and R. C. Ashoori, Science **340**, 1427 (2013).

[20] M. Gibertini, A. Singha, V. Pellegrini, M. Polini, G. Vignale, and A. Pinczuk, Phys. Rev. B **79**, 241406(R) (2009).

[21] C.-H. Park and S. G. Louie, Nano Lett. **9**, 1793 (2009).

[22] L. Brey, H. A. Fertig, R. Côté, and A. H. MacDonald, Phys. Rev. Lett. **75**, 2562 (1995).

[23] R. Côté, A. H. MacDonald, L. Brey, H. A. Fertig, S. M. Girvin, and H. T. C. Stoof, Phys. Rev. Lett. **78**, 4825 (1997).

[24] D. K. Maude, M. Potemski, J. C. Portal, M. Henini, L. Eaves, G. Hill, and M. A. Pate, Phys. Rev. Lett. **77**, 4604 (1996).

[25] R. Côté and A. H. MacDonald, Phys. Rev. Lett. **65**, 2662 (1990); Phys. Rev. B **44**, 8759 (1991).

[26] P. K. Lam and S. M. Girvin, Phys. Rev. B **30**, 473 (1984).

[27] K. Moon, H. Mori, K. Yang, S. M. Girvin, A. H. MacDonald, L. Zheng, D. Yoshioka, and S.-C. Zhang, Phys. Rev. B **51**, 5138 (1995).

[28] C. Kallin and B. I. Halperin, Phys. Rev. B **30**, 5655 (1984); Y. A. Bychkov, S. V. Iordanskii, and G. M. Eliashberg, Pis'ma Zh. Eksp. Teor. Fiz. **33**, 152 (1981) [JETP Lett. **33**, 143 (1981)].

[29] Y. A. Bychkov, T. Maniv, I. D. Vagner, and P. Wyder, Phys. Rev. Lett. **73**, 2911 (1994).

[30] R. Côté, J. P. Fouquet, and W. Luo, Phys. Rev. B **84**, 235301 (2011).

[31] V. M. Apalkov and T. Chakraborty, Phys. Rev. Lett. **112**, 176401 (2014); A. Ghazaryan and T. Chakraborty, Phys. Rev. B **91**, 125131 (2015).

[32] W. Luo and T. Chakraborty, J. Phys.: Condens. Matter **28**, 015801 (2016).